#### **RESEARCH**



# Accuracy of full arch scans performed with nine different scanning patterns— an in vitro study

Kerstin Schlögl<sup>1</sup> · Jan-Frederik Güth<sup>2</sup> · Tobias Graf<sup>2</sup> · Christine Keul<sup>1</sup>

Received: 8 August 2024 / Accepted: 8 January 2025 / Published online: 27 January 2025 © The Author(s) 2025, corrected publication 2025

#### **Abstract**

Objective Evaluation of the accuracy of direct digitization of maxillary scans depending on the scanning strategy.

Materials and methods A maxillary model with a metal bar as a reference structure fixed between the second molars was digitized using the CEREC Primescan AC scanner (N=225 scans). Nine scanning strategies were selected (n=25 scans per strategy), differing in scan area segmentation (F=full jaw, H=half jaw, S=sextant) and scan movement pattern (L=linear, Z=zig-zag, C=combined). Trueness was assessed by evaluating linear differences in the X, Y, and Z axes and angular deviations ( $\alpha$  axial,  $\alpha$  coronal,  $\alpha$  total) compared to a reference dataset. Statistical differences were analyzed using Kruskal-Wallis and Mann-Whitney U tests (p<0.017). Precision was analyzed by the standard deviation of linear and angular aberrations (ISO 5725-1) (p<0.05).

**Results** Strategy  $F_L$  showed significantly higher trueness and precision than  $F_Z$  for VE (p=0.009),  $V_E(y)$  (p=0.010),  $\alpha_{\text{overall}}$  (p=0.004), and  $\alpha_{\text{axial}}$  (p=0.002). Strategy  $F_C$  demonstrated significantly better trueness than  $F_Z$  for VE (p=0.007),  $\alpha_{\text{overall}}$  (p=0.010), and  $\alpha_{\text{coronal}}$  (p=0.013). For scan segmentation,  $F_L$  showed better trueness for  $V_E(y)$  (p=0.001) and  $\alpha_{\text{axial}}$  (p<0.001) than  $H_L$ . Strategy  $H_L$  showed better trueness for  $V_E(z)$  than for  $F_L$  and  $S_L$  (p=0.001, p=0.002). The scanning patterns  $F_L$ ,  $F_C$ , and  $H_L$  exhibited the best performance for trueness and precision.

**Conclusions** Scanning motion and segmentation have a significant impact on the trueness and precision of full-arch scans. **Clinical relevance** The scanning strategy is decisive in enhancing the clinical workflow and the accuracy of full-arch scans.

Keywords Full-arch digitization · Scanning strategies · Accuracy · Intraoral scanner

#### Introduction

The digital workflow in dentistry has recently been transformed by the influence of computer-aided design (CAD) and computer-aided manufacturing (CAM) across nearly all clinical applications, such as orthodontics and prosthodontics. Modern digital technologies in dentistry now provide enhanced efficiency and superior quality in diagnostics, clinical monitoring, therapy planning, and restoration

fabrication. Additionally, the standardization achieved through digital workflows reduces inaccuracies associated with conventional impression-taking and model fabrication [1]. Furthermore, documentation through direct digitization facilitates [1]more objective treatment decisions by relying on acquired diagnostic data [2, 3].

A complete digital workflow without the process of a conventional impression involves three coordinated steps: data acquisition, data processing, and restoration fabrication [4]. The accuracy of the scan, and consequently the data acquisition process, plays a decisive role in this initial step of the digital workflow, as the subsequent steps depend on the quality of this data. Several factors can influence this accuracy. In this context the scanning system and its calibration [5], experience of the operator [6] and the scanning strategy [7, 8] are critical determinants of the accuracy, in detail the trueness and precision of the resulting model data.

For evaluating the accuracy of full-jaw datasets, there is currently no standardized guideline available. Up to

Published online: 27 January 2025



Department of Prosthetic Dentistry, LMU University Hospital, LMU Munich, Goethestrasse 70, 80336 Munich, Germany

Department of Prosthetic Dentistry, Center for Dentistry and Oral Medicine (Carolinum), Goethe University Frankfurt am Main, Frankfurt am Main, Germany

date, two methods are described in the literature. The first involves using a best-fit algorithm to superimpose test and reference data, allowing the calculation of metric deviations between the two datasets [9–11]. However, this method is limited by potential unrecognized misalignments introduced by the software algorithm during the alignment process. The second method uses metrical analysis of real geometric values obtained from reference objects, which are either fixed to an in vitro analysis model or attached to the patient's arch in vivo [12–16].

The current consensus in literature is that the new generation of intraoral scanners demonstrate convincing accuracy for scans up to a quadrant, with equivalent or even superior accuracy of the generated virtual dental model [9]. However, scanning an entire jaw remains challenging [15, 17] as increased scan distances are associated with cumulative scanning and merging errors, resulting in higher inaccuracies, particularly for full-arch scans [18]. Notably, these inaccuracies depend on the specific systems utilized [19, 20].

Considering this, the question arises how potential sources of error in the scanning strategy affect the trueness and precision of digital data acquisition. Several studies indicate that accuracy improves with a more complex, non-linear scanning strategy [8, 21, 22], while others recommend adhering to the use of manufacturer's suggested strategy [23]. Additionally, capturing undercuts requires rotation of the handpiece to enhance detection [15].

The aim of the present study is to systematically investigate the influence of different movement patterns and targeted scan segmentation on scan accuracy. This study evaluates trueness and precision in the in-vitro digitization of a maxillary model using a new generation IOS scanner (CEREC Primescan AC). The null hypothesis is that varying the scanning pattern will not result in significant differences intrueness or precision.

#### **Materials and methods**

A maxillary full-arch model made of polyurethane (AlphaDie MF, LOT 2012008441; Schütz Dental GmbH, Rosbach, Germany) with a homogeneous, matt surface was used as analysis model to conduct the study. A metal bar was inserted in the area of the second molars and used as a reference structure (GARANT, DIN 875-00-g; Hoffmann Group, Munich, Germany).

#### Acquisition of the reference dataset of the bar

The reference measurement of the metal bar was carried out with a coordinate measuring machine (CMM: Mitutoyo Crysta Apex C 574; Createch Medical Mendaro, Spain; software: MCOSMOS Mitutoyo Software; Mitutoyo, Neuss, Germany) before it was fixed on the analysis model. This measurement was performed at a temperature of 20 °C with a maximum permissible error (MPEe) of the CMM of 1.9  $\mu$ m + (3\*L/1000), where the parameter L is defines by the real length of the used metal bar. Subsequently, the STL dataset generated by the CMM was imported into the analysis software (Geomagic Control 2015; version: 2015.3.1.0, 64-bit, Geomagic, Morrisville, MC, US). The calculated reference length of the metal bar was 55.066 mm.

# Scanning of the upper jaw model

CEREC Primescan AC (software version 2015.3.1.0, Dentsply Sirona, Bensheim, Germany) was used for all scans (n=25/strategy). Nine different scanning strategies were developed for direct digitization, combining the segmentation of the scan area (F=full jaw, H=half jaw, and S=Sextant) and three different scan movement patterns ( = linear, z = zig-zag, and c = combined) as shown in Fig. 1. During the scan, it was ensured that a maximum of 20 mm of the bar ends were captured by the scanner to avoid connection of the complete bar in the virtual dataset. The full length of the bar was not scanned, due to the following reason: The reference bar contains no geometric structures for optimal merging the single captures of CEREC Primescan AC. Hence, the digitization of the complete bar was not possible without causing distortions in the complete arch scan, as the software algorithm of CEREC Primescan AC tried to connect both bar ends if the scanning area was too large.

An experienced operator [K.S.] performed all scans using the extraoral data acquisition mode of CEREC Primescan AC. Each scan was obtained under the same conditions with constant ambient light settings. At the beginning of each scan, the CEREC Primescan AC scanning device was calibrated using the "Calibration Set Primescan" according to manufacturer's guidelines. A maximum of two scans were performed successively with a following break of 30 min, so that any influence by heating of the scanning device could be excluded.

# Data analysis and calculation of the parameters (linear parameters/angular parameters)

Each scan (N=225, n=25 per group) was exported as an STL dataset from the respective scan software of CEREC Primescan AC and imported into the analysis software (Geomagic Control 2015). The data was virtually adjusted in a three-dimensional coordinate system, that included XZ-, XY-, and YZ-axes as the coronal, transversal and sagittal planes (Fig. 2). Using the "Contact Feature" mode of



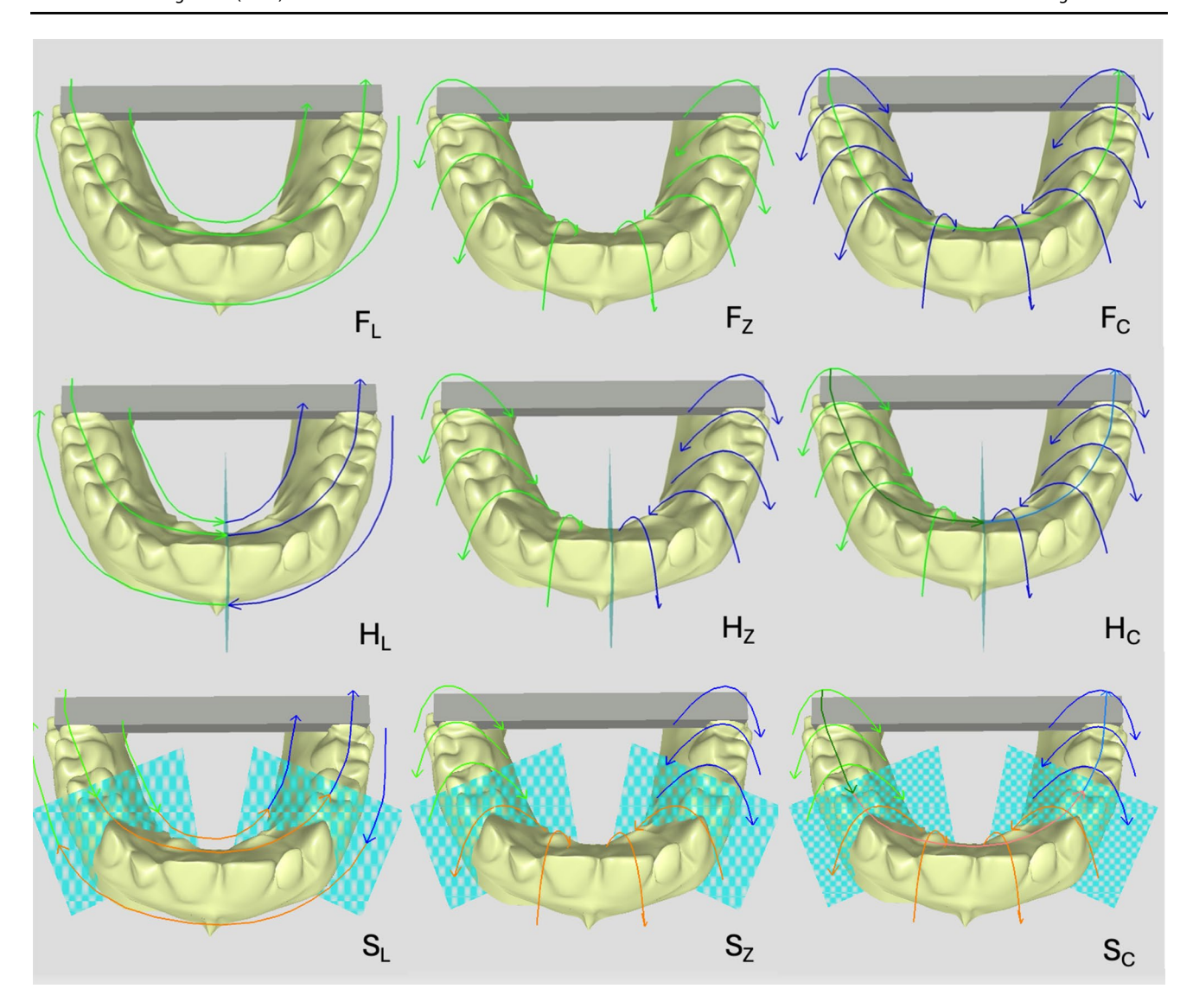


Fig. 1 Visualization of the scanning strategies

the analysis software, anterior surfaces (AP 1 and AP 2), posterior surfaces (PP 1 and PP 2), and vestibular surfaces (VP 1 and VP 2) were constructed at each bar end (Fig. 2).

By the intersection of the planes further vectors and points were defined: the intersection lines of the anterior and posterior surfaces resulted in the horizontal vectors  $\vec{V}$  1 (AP1 and PP1) and  $\vec{V}$ 2 (AP2 and PP2). The points P1 and P2 were determined as the intersections of  $\vec{V}$ 1 and VP1 or  $\vec{V}$ 2 and VP2, respectively (Fig. 3). For the metric analysis of the torsion in all three dimensions, the vestibular surface of the second quadrant (VP2) was parallel shifted by the calculated reference length of the metal bar (L=55.066 mm) in the direction of the first quadrant to construct the surface VP2'. The surface VP2' with the vector  $\vec{V}$ 2 resulted in the constructed point P2'. To calculate the metric values of the torsion in the X-, Y- and Z- axes, the vectorial error  $\vec{V}_E$ 

between P2' and P1 was then analyzed using the calculation formula below (x, y, and z are the coordinates of the X-, Y-, and Z-axes):

$$\vec{V}_E = \left( \begin{array}{cc} x_{p1} - & x_{p2} \\ y_{p1} - & y_{p2} \\ z_{p1} - & z_{p2} \end{array} \right)$$

To determine the angular deviations of the upper bar edges,  $\alpha_{\text{overall}}$  was first calculated as follows:

$$\begin{split} &\alpha_{\text{overall}} = \\ &\alpha\cos\frac{X_{V1}*X_{V2} + Y_{V1}*Y_{V2} + Z_{V1}*Z_{V2}}{\sqrt{X_{V1}^2 + Y_{V1}^2 + Z_{V1}^2}*\sqrt{X_{V2}^2 + Y_{V2}^2 + Z_{V2}^2}} \\ &*\frac{180}{Z_{V1}} \end{aligned}$$



Fig. 2 Construction of the surfaces in contact feature mode

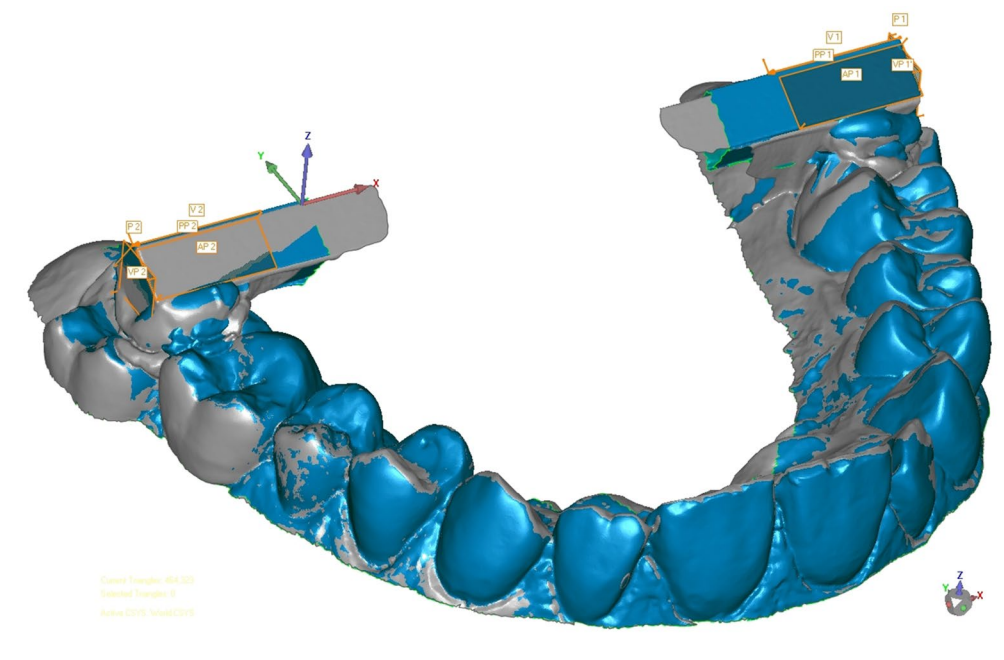
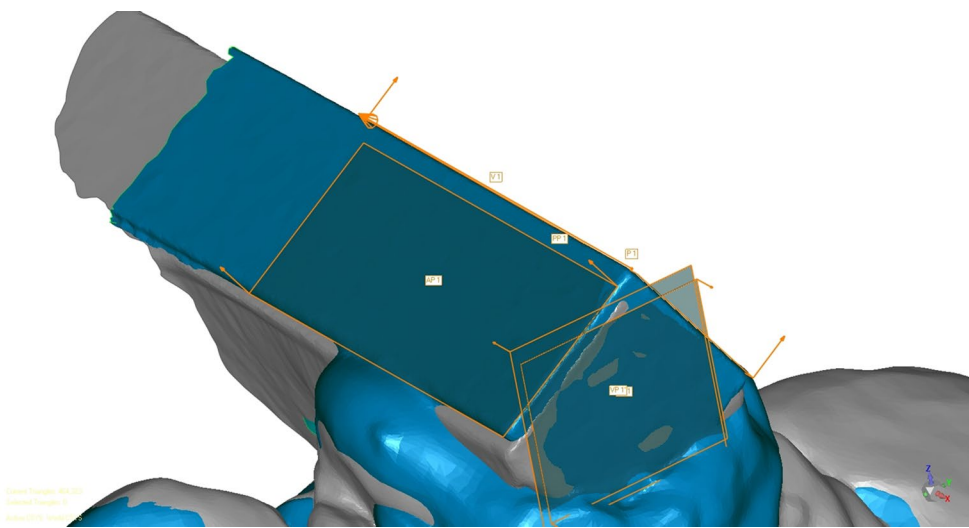


Fig. 3 Construction of the surfaces in the first quadrant



In addition, the differentiated projection of  $\alpha_{overall}$  on the coronal and horizontal planes gives further information about the direction of the angular torsion of the bar. It was calculated using the following equations (x, y, and z are the coordinates of the X-, Y-, and Z-axes):

$$\alpha \; \text{coronal} \; = \; \alpha \; \text{cos} \; \; \frac{X_{V1} * X_{V2} + Y_{V1} * Y_{V2}}{\sqrt{{X_{V1}}^2 + {Y_{V1}}^2} \; * \; \sqrt{{X_{V2}}^2 + {Y_{V2}}^2}} \; * \; \frac{180}{\pi}$$

$$\alpha \, \mathrm{axial} \, = \, \alpha \, \mathrm{cos} \, \, \frac{X_{V1} * X_{V2} + Z_{V1} * Z_{V2}}{\sqrt{{X_{V1}}^2 + {Z_{V1}}^2} * \, \sqrt{{X_{V2}}^2 + {Z_{V2}}^2}} \, * \, \frac{180}{\pi}$$

#### Statistical analysis

Statistical data analysis was performed using SPSS statistics software (version 26.0.0.0, IBM, Armonk, NY, USA). The

significance level was set at 5% (p<0.05). The Kolmogorov Smirnov and Shapiro-Wilk test was performed to assess the normal distribution.

To determine differences in the trueness between the scanning strategies (segmentation and movement), Kruskal-Wallis and the Mann-Whitney-U test with Bonferroni correction (p<0.017) were used. For the analysis of precision (according to ISO 5725-1) the standard deviation was used [13].

### **Results**

The deviations are expressed as median, minimum, maximum and standard deviation in Tables 1 and 2 including the 95% confidence interval for each parameter. The boxplots of all tested strategies are displayed in Figs. 4 and 5.



**Table 1** Descriptive statistics of linear deviations with mean values (M), standard deviation (SD), median (MD) and 95% confidence interval (CI) of CEREC Primescan AC; uppercase superscript letters indicate significant differences between the scanning strategies regarding the trueness; lowercase superscript letters indicate significant differences between the scanning strategies regarding the precision

		ΔL (μm)	VE (μm)	$VE(x) (\mu m)$	VE(y) (µm)	VE(z) (µm)
Strategy FL	M	-64.94	171.53	-67.92	-34.46	121.22
	SD	58.84	59.41	59.03	60.58	75.32
	MIN	-169.07	49.77	-173.24	-126.79	(-59.77)
	MED	-61.67 <sup>A, a</sup>	181.65 <sup>A, C, a</sup>	-65.13 <sup>A, a</sup>	-44.12 <sup>A, a</sup>	127.89 <sup>A, a</sup>
	MAX	60.95	288.59	60.24	78.16	272.12
	95% CI	-89.24/-40.65	147.00/196.05	-92.28/-43.56	-59.46/-9.45	90.13/152.32
Strategy FZ	M	-66.59	301.86*	-50.30	41.59*	148.29
<i></i>	SD	92.73	215.91	95.53	256.96	184.96
	MIN	-261.60	52.45	-262.30	-642.98	-360.63
	MED	-59.09 <sup>A, a</sup>	242.12 <sup>B, a</sup>	-61.57 <sup>A, a</sup>	47.96 <sup>B, a</sup>	159.20 <sup>A, B, a</sup>
	MAX	152.92	945.63	243.22	940.55	539.82
	95% CI	-104.87/-28.31	212.74/390.99	-89.73/-10.86	-64.47/147.66	71.94/224.64
Strategy FC	M	-63.45	175.91*	-61.31	-53.01*	26.16
	SD	73.98	88.16	80.35	132.94	91.23
	MIN	-208.70	43.61	-209.81	-439.21	-141.91
	MED	-65.38 <sup>A, a</sup>	151.6 <sup>C, A, a</sup>	-65.42 <sup>A, a</sup>	-26.40 <sup>A, B, a</sup>	21.67 <sup>B, a</sup>
	MAX	97.88	443.0	96.66	137.00	225.42
	95% CI	-93.99/-32.90	139.52/212.31	-94.48/-28.14	-107.89/1.86	-11.51/63.82
Strategy HL	M	-49.94	182.13*	-50.10	68.91*	12.97
strategy IIE	SD	46.27	116.81	46.27	163.53	107.61
Strategy HZ	MIN	-134.28	44.50	-135.1	-313.18	-185.56
	MED	-41.74 <sup>A, a</sup>	164.63 <sup>A, a</sup>	-42.44 <sup>A, a</sup>	68.7 <sup>A, a</sup>	2.77 <sup>A, a</sup>
	MAX	33.76	524.96	33.41	484.95	186.92
	95% CI	-69.04/-30.82	133.91/230.36	-69.20/-31.00	1.42/136.41	-31.45/57.39
Strategy H7	9370 C1 M	-79.20	303.54*	-81.18*	147.89*	153.65
onategy 112	SD	96.24	237.87	99.16	241.0	174.42
	MIN	-304.23	45.93	-334.15	-157.98	-145.63
	MED	-84.30 <sup>A, a</sup>	192.89 <sup>A, a</sup>	-86.04 <sup>A, a</sup>	56.16 <sup>A, a</sup>	130.41 <sup>B, a</sup>
	MAX	70.98	1016.27	71.23	827.17	541.89
	95% CI	-118.94/-39.46	205.35/401.74	-122.11/-40.24	48.42/247.36	81.65/225.64
Strategy HC	93% CI M	-85.08	216.37*	-83.54	41.15	45.81*
Strategy HC	SD	61.04	120.51	67.58	141.54	165.74
			75.88	-235.46		
	MIN	-236.11	210.34 <sup>A, a</sup>		-263.70	-436.34 <b>31.84</b> <sup>A, B, a</sup>
	MED	-84.32 <sup>A, a</sup>		-85.03 <sup>A, a</sup>	34.34 <sup>A, a</sup>	
	MAX	16.72	584.13	102.13	279.91	522.57
a	95% CI	-110.28/-59.87	166.62/266.12	-111.44/-55.64	-17.28/99.57	-22.61/114.23
Strategy SL	M	-76.23	205.54*	-74.59	19.34*	127.60
	SD	67.11	143.63	73.25	149.18	117.78
	MIN	-258.54	44.94	-266.69	-133.18	-125.56
	MED	-92.44 <sup>A, a</sup>	164.93 <sup>A, a</sup>	-93.13 <sup>A, a</sup>	-24.96 <sup>A, a</sup>	123.22 <sup>A, a</sup>
	MAX	74.67	803.07	78.61	601.37	460.59
	95% CI	-103.94/-48.53	146.25/264.83	-104.83/-44.35	-42.24/80.92	78.98/176.22
Strategy SZ	M	-86.05*	322.01*	-89.07*	115.89*	77.71*
	SD	132.44	313.47	132.91	283.71	282.10
	MIN	-448.36	33.68	-446.19	-204.45	-1037.96
	MED	-60.13 <sup>A, a</sup>	177.74 <sup>A, a</sup>	-62.45 <sup>A, a</sup>	6.53 <sup>A, a</sup>	112.88 <sup>A, a</sup>
	MAX	155.07	1123.22	154.87	923.66	474.73
Strategy SC	95% CI	-140.72/-31.37	192.61/451.41	-143.93/-34.30	-1.23/232.99	-38.74/194.15
Strategy SC	M	-86.66	238.95	-77.72	10.97	43.48*
	SD	67.27	142.08	88.11	208.04	142.25
	MIN	-233.82	50.79	-234.56	-553.95	-442.04
	MED	-79.58 <sup>A, a</sup>	215.08 <sup>A, a</sup>	-82.15 <sup>A, a</sup>	-3.16 <sup>A, a</sup>	62.36 <sup>A, a</sup>
	MAX	35.21	575.84	131.88	432.82	223.60
	95% CI	-114.43/-58.88	180.30/297.61	-114.09/-41.34	-74.90/96.84	-15.24/102.21



Table 2 Descriptive statistics of angle measurements with mean values (M), standard deviation (SD), median (MD) and 95% confidence interval (CI) of CEREC Primescan AC; uppercase superscript letters indicate significant differences between the scanning strategies regarding the trueness; lowercase superscript letters indicate significate differences between the scanning strategies regarding the trueness; lowercase superscript letters indicate significate differences between the scanning strategies regarding the trueness; lowercase superscript letters indicate significant differences between the scanning strategies regarding the trueness; lowercase superscript letters indicate significant differences between the scanning strategies regarding the trueness; lowercase superscript letters indicate significant differences between the scanning strategies regarding the trueness; lowercase superscript letters indicate significant differences between the scanning strategies regarding strategies reg regarding the precision

regarding are breaken	Total Am	TOTO													
	Angul	ar measure	Angular measurements overall (°)	all (°)		Angula	ır measure	angular measurements corona	(°)		Angula	Angular measure	ments axial (c	()	
Strategy	SD	M	MED	MIN/MAX 95%	95% CI	SD	M	MED	MIN/MAX	95% CI	SD	M	MED	MIN/MAX	95% CI
FL	0.12	0.21	$0.21^{A, a}$	0.00/0.57	0.15/0.27	0.13	0.17*	$0.14^{A, B, a}$	0.00/0.56	0.11/0.23	90.0	60.0	$0.08^{A, a}$	0.00/0.21	0.05/0.12
FZ	0.50	0.48*	$0.36^{\mathrm{B,a}}$	0.09/2.00	0.26/0.69	0.35	0.33	$0.25^{B, a}$	0.04/1.43	0.18/0.48	0.38	0.32		0.17/1.4	0.15/0.48
FC	0.14	0.23*	$0.22^{A, a}$	69.0/90.0	0.16/0.30	0.10	0.15	$0.16^{A, a}$	0.00/0.31	0.11/0.20	0.15	0.14*	$0.09^{A, B, a}$	89.0/00.0	0.07/0.20
HL	0.19	0.29*	$0.26^{A, a}$	0.08/0.78	0.20/0.37	0.12	0.15	$0.14^{A, a}$	0.01/0.4	0.10/0.21	0.18	0.22*		0.05/0.72	0.14/0.30
HZ	0.21	0.31*	$0.27^{A, a}$	0.08/1.01	0.21/0.40	0.14	0.18*	$0.14^{A, a}$	0.01/0.47	0.11/0.24	0.21	0.22	$0.17^{A, a}$	0.02/0.91	0.12/0.31
НС	0.17	0.29	$0.27^{A, a}$	0.06/0.77	0.20/0.36	0.16	0.20	$0.17^{A, a}$	0.00/0.65	0.13/0.27	0.13	0.17	$0.12^{A, a}$	0.02/0.51	0.11/0.23
$S\Gamma$	0.32	0.32*	$0.23^{A, a}$	0.05/1.59	0.17/0.45	0.15	0.21*	$0.18^{A, a}$	0.03/0.65	0.14/0.27	0.32	0.19*	$0.12^{A, a}$	0.01/1.58	0.04/0.33
ZS	0.36	0.46*	$0.33^{A, a}$	0.07/1.32	0.17/0.66	0.19	0.30	$0.32^{A, a}$	0.01/0.67	0.22/0.38	0.35	0.30	$0.14^{A, a}$	0.01/1.22	0.15/0.45
SC	0.58	0.42*	$0.25^{A, a}$	0.08/2.66	0.17/0.67	0.33	0.26*	$0.21^{A, a}$	0.01/1.56	0.12/0.41	0.49	0.31	$0.16^{A, a}$	0.04/2.16	0.10/0.52

Shapiro-Wilk test resulted in 1 out of 9 normally distributed group for the linear parameter, for the angular parameters 9 out of 9 were not normally distributed. For the trueness, statistically significant differences between the nine different strategies were found. The precision, determined on basis of the standard deviation, showed also differences between tested groups.

# Influence of movement pattern

For parameters  $V_E$  (p=0.008),  $V_E$ (y) (p=0.023),  $\alpha_{overall}$ (p=0.006) and  $\alpha_{\text{axial}}$  (p=0.033), strategy  $F_L$  results in significantly higher trueness than strategy F<sub>Z</sub>. For V<sub>E</sub> (p=0.008),  $\alpha_{\text{overall}}(p=0.006)$  and  $\alpha_{\text{coronal}}(p=0.005)$  strategy F<sub>C</sub> shows significantly better trueness than strategy F<sub>Z</sub>. Considering  $V_E(z)$ , strategy  $F_C$  resulted in better trueness than  $F_1$  and  $H_1$  than  $H_2$  (p < 0.001 to p = 0.011).

For parameters  $V_E$  and  $V_E(y)$  the angular parameters  $\alpha$   $_{\rm overall},~\alpha$   $_{\rm coronal},~\alpha$   $_{\rm axial},$  the significantly better trueness agrees with a better precision. Strategy F<sub>L</sub> indicates a better precision compared to  $F_C$  for  $\stackrel{f}{V}_E(z)$ .

# Influence of scan segmentation

For parameters  $V_E(y)$  (p=0.005) and  $\alpha_{axial}$  (p=0.002), strategy F<sub>L</sub> showed significantly higher trueness than H<sub>L</sub>. For  $V_E(z)$  (p=0.001) strategy  $H_L$  resulted in significantly better trueness than  $F_L$  and  $S_L$ .

Considering parameters  $V_E(y)$  and  $\alpha_{axial}$ , strategy  $F_L$ resulted in better precision than strategy H<sub>I</sub>. For parameter  $V_{\rm F}(z)$  strategy  $H_{\rm I}$  showed better precision than strategy  $S_{\rm I}$ .

# **Discussion**

The present study evaluates the accuracy of CEREC Primescan AC depending on the scanning pattern used for invitro full-arch digitization. The impact of scanning strategy on the digitization accuracy has been demonstrated repeatedly in the literature [7, 21, 24]. To improve comparability, this study systematically combined three distinct motion patterns with three possible segmentations of the upper jaw. Compared to previously published literature, different strategies were defined and investigated. The null hypothesis of the present study, which stated that there would be no significant differences between the applied scanning strategies, has to be rejected, as significant differences could be observed.

For CEREC Primescan AC, two scanning patterns have been shown to be preferable to a third variation, with strategies involving linear movements proving to be



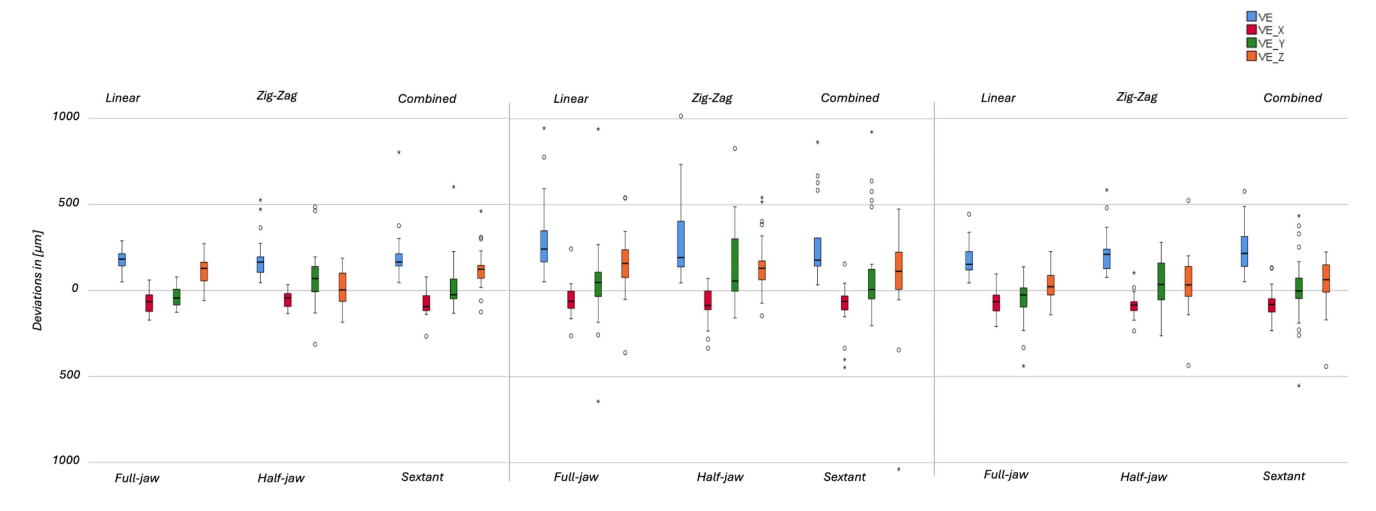


Fig. 4 Statistical analysis of linear deviations

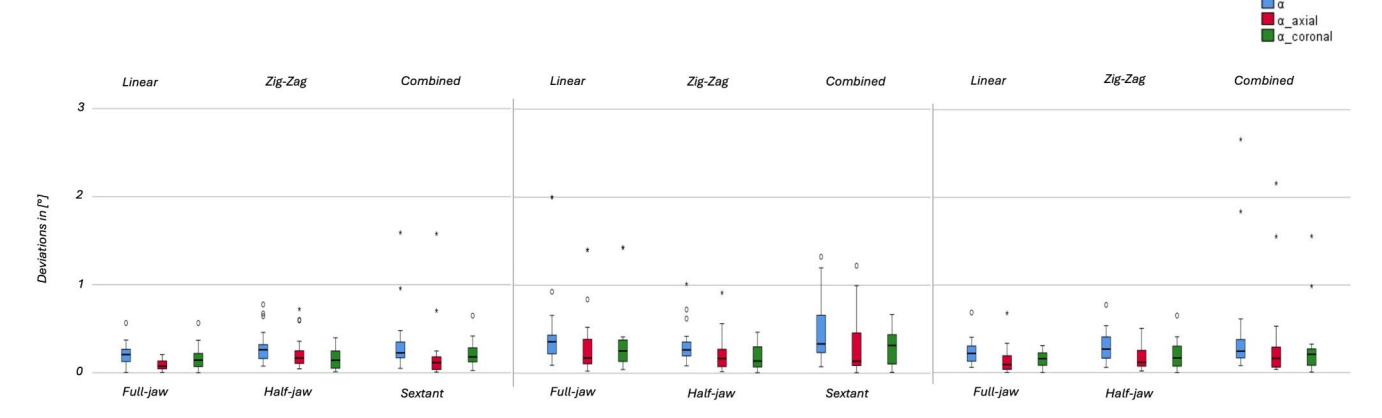


Fig. 5 Statistical analysis of angular deviations

advantageous. Consistent to the present results, Müller et al. [21] recommended the manufacturer's specified scanning protocol, corresponding to strategy  $F_L$  in case of CEREC Primescan AC. Hence, it could be assumed that the constant movements would result in fewer interruptions during image acquisition [8]. Contrary, Passos et al. [8] reported improved accuracy using a strategy that combined linear and rotational movements.

In the present investigation, no significant differences have been observed between the scanning strategies regarding deviations along the X-axis. However, regarding the deviations in the Y- and Z-axes, strategies  $F_C$  and  $F_L$  exhibited a significantly better trueness than strategy  $F_Z$ . Similar results were noted for the angular parameters  $\alpha_{\text{overall}}$ ,  $\alpha_{\text{coronal}}$ , and  $\alpha_{\text{axial}}$ , which were also associated with improved precision. The lower trueness observed with zig-zag movements may be attributed to the absence of occlusal orientation structure, resulting in greater errors caused by inaccurate image overlap [21]. In addition, the varying motion patterns of zig-zag movements could be a disadvantageous due to

the frequent change of the focal plane of the optical acquisition unit. This interpretation aligns with findings reported in the existing literature [8].

The trueness and precision for VE (y) and  $\alpha_{axial}$  of strategy F<sub>L</sub> were superior compared to strategy H<sub>L</sub>. Strategy F<sub>I</sub> aligns with the manufacturer's recommendation but involves the longest scan path distance in one turn. Thus, it can be assumed that a lower number of handpiece rotations may result in reduced interference during data acquisition [8]. Related to the Y-axis, it is conceivable that the scanning errors in the anterior-posterior direction accumulate due to the larger scan section. [19]. Supporting this presumption, Waldecker et al. [25] reported that linear deviations increase with the scanning path length. By dividing the jaw into minor sections of two or three segments, the authors of the present study aimed to minimize the accumulated error of the large scan segment within a complete dental arch. These findings can, with the present study, only be partially confirmed.



For the parameter  $V_E(z)$ , the strategy  $H_L$  demonstrated higher accuracy than the strategies  $F_L$  and  $S_L$ . Similar findings were reported in a study using CEREC Omnicam (Dentsply Sirona, Bensheim, Germany) where strategy  $H_L$  also produced the best results in this context [22]. Nevertheless, as CEREC Omnicam and CEREC Primescan employ entirely different camera technologies, this comparison requires validation through testing with the same scanner model.

In the present study, accuracy was determined as trueness and precision according to ISO 5725-1 [26] and prior literature [13, 27]. According to this definition, trueness was assessed using the mean values of the linear and angular deviations between the test and reference data, while precision was estimated based on the standard deviation (SD). This was due to using actual one-dimensional measurements for a predefined geometric structure (the bar) rather than relying on best-fit alignments of the test dataset for the bar or the complete arch. Linear measurements were performed along the X-, Y-, and Z-axes, allowing for a more accurate assessment of the subsequent intraoral fit of the restoration. The successful in vivo application of this method has also been documented [13].

However, like every scientific work, the present work is subjected to several limitations.

It should be noted that this study investigates only the initial stage of the digital workflow. The accuracy of the fabricated prosthesis is influenced by several factors, including the number of interfaces, the CAD and the CAM of the restoration [28, 29]. For fixed prostheses, particularly those extending to a full arch, digitization plays a pivotal role by influencing linear and angular deviations, potentially resulting in restoration misfits. Unlike tooth-supported restorations, implant-supported restorations attached to osseo-integrated implants lack the ability to compensate for these inaccuracies.

In this study, CEREC Primescan AC, a currently available model on the market, was used. The scanner employs a light optical measurement principle based on triangulation in combination with confocal principle to generate three-dimensional surface data [30]. As the dimension of the IOS handpiece may limit the application of the rotating/zig-zag scanning strategy in the molar region, a clinical trial is necessary for further investigation. Moreover, maintaining a complex scanning path such as "zig-zag" is more difficult in vivo than when scanning a model.

Since intraoral conditions - such as saliva, limited space, handling of soft tissues, light variations, and patient movements - are proven to affect the accuracy of IOS data [20, 24], further research focusing on full-arch scans under clinical conditions should be prioritized. Besides, for a more patient-like configuration, it would make sense to fix the

reference object in the occlusal plane to be in the same focal plane and include more than one operator for the performance of the scans. CEREC Primescan AC offers an extraoral mode that was used for our in-vitro scans that could also be an influencing parameter on the generated data. According to Kuhr et al. [31], the scanning of the maxillary model results in the advantage of a larger surface area in the palatal region, which can be used as an orientation structure. Due to the anatomical shape of the model with physiologically shaped teeth, the study design is like a clinical setup. Therefore, future studies should incorporate adjusted scanning strategies in a clinical setup, include more scanning operators, and evaluate scanning devices from other manufacturers to provide comprehensive insights.

For CEREC Primescan AC the scanning pattern  $F_L$ ,  $F_C$ , and  $H_L$  exhibited the best performance for trueness and precision. Overall, the findings of the current investigations suggest that linear and combined movements in combination with full jaw or half jaw segmentation (strategies  $F_L$ ,  $F_C$ , and  $H_L$ ) are advantageous for CEREC Primescan AC regarding trueness and precision.

# **Conclusions**

Within the limitations of this study, it can be concluded that:

- the combination of full arch with the linear or combined movement pattern (strategies F<sub>L</sub> and F<sub>C</sub>) resulted in better trueness and precision for most measured parameters compared to the zig-zag movement (F<sub>7</sub>).
- the linear motion pattern in combination with full-arch or half-jaw segmentation (strategies F<sub>L</sub>, H<sub>L</sub>) showed significantly better trueness compared to sextant segmentation (S<sub>L</sub>) for linear measurement parameters.

Thus, scanning movement and scan segmentation have a significant influence in trueness and precision of full-arch scans. However, for clear recommendations of ideal scan paths for the clinical practice, further studies should be carried out.

**Author contributions** J-F.G. developed the theoretical framework and study conception. C.K. and J-F.G. contributed the study design. K.S. carried out the experiments. C.K. performed the statistical analysis and performed the analysis and interpretation of the results together with K.S.K.S. wrote the manuscript and designed the figures and tables with support from J-F.G. and C.K.C.K., K.S., J-F.G. and T.G. reviewed the final version of the manuscript.K.S. did the final approval of the manuscript.

Funding Open Access funding enabled and organized by Projekt DEAL.

Data availability No datasets were generated or analysed during the current study.



#### **Declarations**

**Ethical approval** This article does not contain any studies with human participants or animals performed by any of the authors.

**Competing interests** The authors declare no competing interests.

**Open Access** This article is licensed under a Creative Commons Attribution 4.0 International License, which permits use, sharing, adaptation, distribution and reproduction in any medium or format, as long as you give appropriate credit to the original author(s) and the source, provide a link to the Creative Commons licence, and indicate if changes were made. The images or other third party material in this article are included in the article's Creative Commons licence, unless indicated otherwise in a credit line to the material. If material is not included in the article's Creative Commons licence and your intended use is not permitted by statutory regulation or exceeds the permitted use, you will need to obtain permission directly from the copyright holder. To view a copy of this licence, visit http://creativecommons.o rg/licenses/by/4.0/.

# References

- Güth JF, Runkel C, Beuer F, Stimmelmavr M, Edelhoff D, Keul C (2017) Accuracy of five intraoral scanners compared to indirect digitalization. Clin Oral Investig 21:1445-1455
- Kühne C, Lohbauer U, Raith S, Reich S (2021) Measurement of tooth wear by means of digital impressions: an in-vitro evaluation of three intraoral scanning systems. Appl Sci 11:5161
- Suese K (2020) Progress in digital dentistry: the practical use of intraoral scanners. Dent Mater J 39:717-722
- Schweiger J, Kieschnick A (2020) CAD/CAM in digital dentistry. teamwork media GmbH
- 5. Rehmann P, Sichwardt V, Wöstmann B (2017) Intraoral scanning systems: need for maintenance. Int J Comput Dent 20:367-373
- Resende CCD, Barbosa TAQ, Moura GF, Tavares LN, Rizzante FAP, George FM, Neves FD, Mendonça G (2021) Influence of operator experience, scanner type, and scan size on 3D scans. J Prosthet Dent 125:294-299
- Mai HY, Lee CH, Lee KB, Kim SY, Lee JM, Lee KW, Lee DH (2022) Impact of scanning strategy on the accuracy of completearch intraoral scans: a preliminary study on segmental scans and merge methods. J Adv Prosthodont 14:88-95
- Passos [19] L, Meiga S, Brigagão V, Street A (2019) Impact of different scanning strategies on the accuracy of two current intraoral scanning systems in complete-arch impressions: an in vitro study. Int J Comput Dent 22:307-319
- Schmidt A, Benedickt CR, Schlenz MA, Rehmann P, Wöstmann B (2021) Accuracy of four different intraoral scanners according to different preparation geometries. Int J Prosthodont 34:756-762
- Ender A, Mehl A (2015) In-vitro evaluation of the accuracy of conventional and digital methods of obtaining full-arch dental impressions. Ouintessence Int 46:9-17
- 11. Ender A, Mehl A (2011) Full arch scans: conventional versus digital impressions—an in-vitro study. Int J Comput Dent 14:11-21
- 12. Güth JF, Edelhoff D, Schweiger J, Keul C (2016) A new method for the evaluation of the accuracy of full-arch digital impressions in vitro. Clin Oral Investig 20:1487-1494
- 13. Keul C, Güth JF (2020) Accuracy of full-arch digital impressions: an in vitro and in vivo comparison. Clin Oral Investig 24:735–745

- 14. Schmidt A, Benedickt CR, Schlenz MA, Rehmann P, Wöstmann B (2020) Torsion and linear accuracy in intraoral scans obtained with different scanning principles. J Prosthodont Res 64:167-174
- 15. Schlenz MA, Stillersfeld JM, Wöstmann B, Schmidt A (2022) Update on the accuracy of conventional and digital full-arch impressions of partially edentulous and fully dentate jaws in young and elderly subjects: a clinical trial. J Clin Med 11:3723
- Kontis P, Güth JF, Keul C (2022) Accuracy of full-arch digitalization for partially edentulous jaws-a laboratory study on basis of coordinate-based data analysis. Clin Oral Investig 26:3651-3662
- 17. Winkler J. Gkantidis N (2020) Trueness and precision of intraoral scanners in the maxillary dental arch: an in vivo analysis. Sci Rep 10:1-11
- 18. Ahn JW, Park JM, Chun YS, Kim M (2016) A comparison of the precision of three-dimensional images acquired by 2 digital intraoral scanners: effects of tooth irregularity and scanning direction. Korean J Orthod 46:3-10
- 19. Ender A, Zimmermann M, Mehl A (2019) Accuracy of completeand partial-arch impressions of actual intraoral scanning systems in vitro. Int J Comput Dent 22:11-19
- 20. Keul C, Güth JF (2022) Influence of intraoral conditions on the accuracy of full-arch scans by Cerec Primescan AC: an in vitro and in vivo comparison. Int J Comput Dent 25:17–25
- 21. Müller P, Ender A, Joda T, Katsoulis J (2016) Impact of digital intraoral scan strategies on the impression accuracy using the TRIOS pod scanner. Quintessence Int 47:343-349
- Medina-Sotomayor P, Pascual MA, Camps AI (2018) Accuracy of four digital scanners according to scanning strategy in complete-arch impressions. PLoS ONE 13:e0202916
- Ender A, Mehl A (2013) Influence of scanning strategies on the accuracy of digital intraoral scanning systems. Int J Comput Dent
- 24. Ender A, Attin T, Mehl A (2016) In vivo precision of conventional and digital methods of obtaining complete-arch dental impressions. J Prosthet Dent 115:313-320
- Waldecker M, Rues S, Behnisch R, Rammelsberg P, Bömicke W (2022) Effect of scan-path length on the scanning accuracy of completely dentate and partially edentulous maxillae. J Prosthet
- 26. International Organization for Standardization (1994) Accuracy (trueness and precision) of measurement methods and resultspart 1: General principles and definitions (ISO 5725-1:1994). ISO, Geneva
- 27. Mehl A, Reich S, Beuer F, Güth JF (2021) Accuracy, trueness, and precision—a guideline for evaluation of these basic values in digital dentistry. Int J Comput Dent 24:341-352
- 28. Nedelcu RG, Persson AS (2014) Scanning accuracy and precision in 4 intraoral scanners: an in vitro comparison based on 3-dimensional analysis. J Prosthet Dent 112:1461-1471
- 29. Ferrini F, Sannino G, Chiola C, Capparé P, Gastaldi G, Gherlone EF (2019) Influence of intraoral scanner (IOS) on the marginal accuracy of CAD/CAM single crowns. Int J Environ Res Public Health 16:544
- Tewes M, Berner M (2020) Device, method and system for generating dynamic projection patterns in a confocal camera. Google Patents
- Kuhr F, Schmidt A, Rehmann P, Wöstmann B (2016) A new method for assessing the accuracy of full arch impressions in patients. J Dent 55:68-74

Publisher's note Springer Nature remains neutral with regard to jurisdictional claims in published maps and institutional affiliations.

